

Journal of Experimental Botany, Vol. 73, No. 9 pp. 2937–2951, 2022 https://doi.org/10.1093/jxb/erac062 Advance Access Publication 17 February 2022

This paper is available online free of all access charges (see https://academic.oup.com/jxb/pages/openaccess for further details)



TECHNICAL INNOVATION

An efficient LC-MS method for isomer separation and detection of sugars, phosphorylated sugars, and organic acids

Somnath Koley^{1,†,*,}, Kevin L. Chu^{1,2,†,}, Saba S. Gill^{1,2,} and Doug K. Allen^{1,2,*,}

- ¹ Donald Danforth Plant Science Center, St Louis, MO 63132, USA
- ² United States Department of Agriculture-Agriculture Research Service, Donald Danforth Plant Science Center, St Louis, MO 63132, USA
- [†]These authors contributed equally to this work.
- * Correspondence: skoley@danforthcenter.org or doug.allen@ars.usda.gov

Received 24 October 2021; Editorial decision 14 February 2022; Accepted 15 February 2022

Editor: Yuki Nakamura, Academia Sinica, Taiwan

Abstract

Assessing central carbon metabolism in plants can be challenging due to the dynamic range in pool sizes, with low levels of important phosphorylated sugars relative to more abundant sugars and organic acids. Here, we report a sensitive liquid chromatography-mass spectrometry method for analysing central metabolites on a hybrid column, where both anion-exchange and hydrophilic interaction chromatography (HILIC) ligands are embedded in the stationary phase. The liquid chromatography method was developed for enhanced selectivity of 27 central metabolites in a single run with sensitivity at femtomole levels observed for most phosphorylated sugars. The method resolved phosphorylated hexose, pentose, and triose isomers that are otherwise challenging. Compared with a standard HILIC approach, these metabolites had improved peak areas using our approach due to ion enhancement or low ion suppression in the biological sample matrix. The approach was applied to investigate metabolism in high lipid-producing tobacco leaves that exhibited increased levels of acetyl-CoA, a precursor for oil biosynthesis. The application of the method to isotopologue detection and quantification was considered through evaluating ¹³C-labeled seeds from *Camelina sativa*. The method provides a means to analyse intermediates more comprehensively in central metabolism of plant tissues.

Keywords: Central metabolism, ion suppression and enhancement, isomer separation, isotopic labeling, liquid chromatography—mass spectrometry, metabolite quantification, mixed-mode column chromatography, oilseeds.

Introduction

Compared with other global profiling 'omics' approaches, metabolomics offers a direct and comprehensive snapshot of stationary cellular phenotypes (Allwood *et al.*, 2011; Allen,

2016; Fessenden, 2016; Doerr, 2017) and is used as a component of functional genomics (Fiehn *et al.*, 2000; Bino *et al.*, 2004; Fernie *et al.*, 2005; Quanbeck *et al.*, 2012; Schilmiller *et al.*, 2015;

Vallarino et al., 2018; Wu et al., 2018). The profiling and quantification of metabolites can provide a first approximation of what network pathways are metabolically active (Roessner et al., 2001; Daloso et al., 2015; Kim et al., 2015; Liu et al., 2017; Mansfeld et al., 2017). Changes in metabolite level are suggestive if not indicative of changes in metabolism; however, as a pool size measurement is reflective of one time and encompasses all events that led up to the measurement, it is not inherently correlated with metabolic flux through a cell. Changes in metabolite pool sizes may occur without differences in flux, and alternatively more flux through a pathway does not require a particular increase or decrease in steady state metabolite levels. Therefore, to increase understanding in metabolism and resolve complex metabolic networks, stable isotopes (e.g. ¹³C and ¹⁵N) are supplied exogenously and the isotopologues can be similarly quantified as an extension of metabolite analysis (Giavalisco et al., 2011, 2009; de Jong and Beecher, 2012; Fernie and Morgan, 2013; Heise et al., 2014). The incorporation of isotopes provides dynamic information to decipher the altered rates of synthesis or degradation. Generally this is done within steady state metabolism where pools do not change (Allen et al., 2009; Fan et al., 2012; Higashi et al., 2014; Allen, 2016); however, labeling of metabolite pools that are changing in size has also garnered attention (Antoniewicz, 2013).

When isotopes have been used, plant studies have inferred metabolic operation from the labeling directly (Roessner-Tunali et al., 2004; Huege et al., 2007; Hasunuma et al., 2010; Weissmann et al., 2016; Arrivault et al., 2017; Dethloff et al., 2017; Koley et al., 2019; Simpson et al., 2021) or used computational approaches including isotopically stationary metabolic flux analysis (Allen and Young, 2013; Masakapalli et al., 2014b; Tsogtbaatar et al., 2020), isotopically non-stationary metabolic flux analysis (INST-MFA) (Ma et al., 2014; Xu et al., 2021), kinetic flux profiling (Szecowka et al., 2013), or other kinetic approaches (e.g. Colón et al., 2010). Studies have focused on central carbon metabolism, which includes glycolysis, the Calvin-Benson cycle, the pentose phosphate pathway, and the Krebs cycle (Petucci et al., 2016), because central metabolism is the source of metabolic precursors needed for growth, development, and reproduction processes. Dependent on the scientific question and constraints imposed by the plant organ, steady state labeling or transient isotopic labeling may be required (Allen, 2016). Amino acids within proteins can be labeled over long periods of steady state, resulting in quantitative assessments of metabolism in seeds and cells (Allen et al., 2009; O'Grady et al., 2012). However, many tissues have limited durations of isotopic steady state, for example the diurnal photosynthetic metabolism in leaves, which requires INST-MFA approaches (Shastri and Morgan, 2007; Ma et al., 2014, 2017; Xu et al., 2021). The additional information in transient labeling can also be used to infer labeling of atoms and to further postulate about metabolic operation (Arrivault et al., 2017; Allen and Young, 2020; AuBuchon-Elder et al., 2020).

Such transient labeling methods require identification and quantification of isotopologues of intermediates in central metabolism, which are assessed through nuclear magnetic resonance (Kim et al., 2010, 2011; Masakapalli et al., 2014a; Heux et al., 2017; Schwechheimer et al., 2018; Millard et al., 2021) or through mass spectrometry (MS) with electrospray ionization (ESI)-based liquid chromatography tandem mass spectrometry (LC-MS/MS) being the most common approach (Balcke et al., 2014, 2017; Dias et al., 2015; Jorge et al., 2016; Choi and Antoniewicz, 2019; Subbaraj et al., 2019; Czajka et al., 2020). ESI-MS has emerged as an important analytical tool to measure central metabolites like sugars, phosphorylated sugars, and organic acids (Milne et al., 2013). To increase our understanding of dynamic metabolic processes, there remains a need to improve measurements of the intermediates of central pathways accurately (Nöh and Wiechert, 2006; Toya et al., 2010).

The development of ESI technology by Fenn et al. (1989) that could be linked to MS was transformative for studies in metabolism. Liquid chromatography using ESI is a gentle method that is less apt to degrade molecules containing potentially labile groups such as phosphate or thiol bonds while enabling the desolvation of metabolites resulting in ions in the gas phase that could be transferred to the MS. Detecting phosphorylated analytes and other central metabolites is often challenging due to co-eluted metabolites and ion suppression from sample matrices (Kebarle and Tang, 1993; Annesley, 2003; Sarvin et al., 2020). Though many compounds can be resolved by differential mass separation in the MS, key central carbon metabolites consist of different structural isomers such as hexose phosphates (e.g. fructose 6-phosphate, glucose 1-phosphate (G1P), and glucose 6-phosphate (G6P)), pentose phosphates (e.g. ribose 5-phosphate and ribulose 5-phosphate), and triose phosphates (e.g. dihydroxyacetone phosphate (DHAP) and glyceraldehyde 3-phosphate (GAP), or 2-phosphoglycerate (2PGA) and 3-phosphoglycerate (3PGA)) that have equivalent compositions and thus identical masses. As a subset of these isomers are present in individual pathways (e.g. 3PGA, but not its isomer, is an intermediate of the Calvin-Benson cycle in chloroplasts of plant leaves), studies would benefit from resolving the structurally different chemical species. Hence, resolving these isomers with good peak shapes can enrich the understanding of biochemical processes in subcellular compartments.

The number of analytes that can be detected and sensitively quantified can be optimized by considering interactions between analytes and their derivatives with the stationary phase of the column such that elution individually and in a discrete fashion results in resolved sharp peaks with the best signal to noise ratio. Detection of hydrophilic metabolites from reversed-phase chromatography can be challenging because polar molecules have limited retention on the column (Xhaferaj et al., 2020; Iturrospe et al., 2021), which can lead to poor separation. Chemical derivatization techniques have partially overcome this issue (Kwon and Kim, 1993; Castells et al., 2002;

Nordström et al., 2004; Rende et al., 2019; Higashi and Ogawa, 2020), but can be tedious or result in losses due to additional processing, incomplete reactions, or instability. In addition, multiple derivatization reagents are required for central metabolites since they contain a wide range of different chemical groups. Ion-pairing approaches, where a component (e.g. tributylamine) is added to the buffer, can help polar metabolite retention on a reversed-phase column by neutralizing charges (Coulier et al., 2006; Arrivault et al., 2009; Ma et al., 2014, 2017) though ion pairing reagents leave behind a residue that is difficult to remove from the column and LC system even with repeated cleaning. The strong contaminating signal results in ion suppression in subsequent non-ion pairing runs which is problematic when the instrument is not dedicated exclusively for ion pairing use. The contamination can also affect chromatography of other columns and negatively impact instrument performance. More recently, hydrophilic interaction chromatography (HILIC) methods were developed to separate polar compounds using compositionally similar buffers as typical reversed-phase chromatography. Partially water-soluble polar analytes are retained on the hydrophilic stationary phase and eluted by increasing water in the mobile phase. Organic solvent concentrations are higher at the start of the run; thus, the sample must be solubilized in a more organic solution to avoid precipitation upon injection and ensure binding to the column. Solubilization of the sample in greater concentrations of organic phase is not ideal for polar compounds such as phosphorylated sugars, which readily dissolve in more aqueous phases (Johnson et al., 2010; Jandera, 2011), but is necessary for HILIC column binding. Acknowledged poor peak shapes of charged metabolites (especially metal-sensitive analytes) have been reported when using a HILIC column (Myint et al., 2009; Heaton and McCalley, 2016) indicating the tradeoff. Some of the more recent developments with HILIC technology use zwitterionic stationary phases and medronic acid as additives in the buffer at micromolar levels resulting in better separation of isomers and improved peak shapes (Hsiao et al., 2018; Czajka et al., 2020); however, the interaction between highly polar compounds and the zwitterionic hydrophilic stationary phase can be excessively strong and prevent elution resulting in carryover.

Ion exchange chromatography (IEC) provides a sensitive approach for the analysis of phosphorylated compounds and can be better suited for analysing phosphorylated sugars. IEC methods are capable of separating most of the analytes involved in central carbon metabolism with good reproducibility (Kvitvang et al., 2014; Schwaiger et al., 2017; Fan et al., 2018). Buffers for IEC including potassium hydroxide are not generally MS-compatible, and hence additional membrane devices for proton-potassium exchange to prevent potassium hydroxide from entering the MS system and to remove carbonates are required, adding to the cost and maintenance of the system, and detracting from routine use by non-MS specialists. Previously published IEC methods to separate phosphorylated sugars and detect organic acids in a single run have advanced

the field (van Dam et al., 2002; Kiefer et al., 2007; Alonso et al., 2010; Kvitvang et al., 2014; Wang et al., 2014); however, run times can become extensive (42-85 min), reducing throughput and increasing solvent costs. Additionally, most sugars are neutral to weak acids with high dissociation constants of 12-14 (e.g. p K_a of sucrose is 12.62) and thus may be difficult to retain and detect on the same run as other polar central metabolites. To address these methodological issues without compromising sensitivity, a mixed-mode column was used that is typically run as an anion exchange column for analysing organic acids. We established a novel HPLC method for the analysis of a wide range of polar central metabolites by exploring the unique characteristics of this hybrid IEC-HILIC system. The method was validated by comparing high lipid-producing tobacco leaf tissue with wild-type and analysing ¹³C-labeling data from the oilseed camelina (Camelina sativa). The resolution of isomers and sensitive detection of low abundance metabolites resulted in the detection of approximately 27 metabolites and can provide a more complete survey of central carbon metabolism in different plant tissues.

Materials and methods

Chemicals and reagents

All phosphorylated sugar, sugar, organic acid, and amino acid standards analysed were purchased from Sigma-Aldrich (St Louis, MO, USA) as was ammonium acetate (NH₄CH₃CO₂) and ammonium formate (NH₄HCO₂). HPLC-grade acetonitrile (ACN) and methanol (CH₃OH) were obtained from Honeywell Research Chemicals, while formic acid (HCOOH, 88%) was obtained from Aqua Solutions, Inc. (Deer Park, TX, USA) and InfinityLab Deactivator Additive (medronic acid, 5 mM stock) from Agilent Technologies, Inc. (Santa Clara, CA, USA).

Plant growth and collection

Camelina sativa plants (var. Suneson) were cultivated from seed in a greenhouse. The growth conditions were 22/20 °C temperature (day/night), 40–50% relative humidity, and 16 h day/8 h night photoperiod. Day light condition was maintained at minimum 250 µmol m⁻² s⁻¹ coming from a combination of 600 W high pressure sodium and 400 W metal halide bulbs, while the light intensity varied up to 450 μmol m⁻² s⁻¹ on bright days through control by a shade cloth. Fifteen-day-old siliques were harvested for isotopic studies in which entire cut siliques were placed in 5 mM MES medium containing [U-13C]glucose for 6, 8, and 10 h under continuous light with the stem protruding into the medium and the silique above the liquid surface exposed to ambient air conditions consistent with greenhouse growth. Samples were flash-frozen in liquid nitrogen after the culturing period and stored at -80 °C until extraction. Seeds from each camelina silique were dissected on dry ice before sample

Wild-type (Wisconsin 38) and transgenic high lipid-producing (HLP) Nicotiana tabacum plants overexpressing WRINKLED1 (WRI1), acyl-CoA:diacylglycerol acyltransferase1 (DGAT1), OLEOSIN, and LEAFY COTYLEDON2 (LEC2) (Vanhercke et al., 2017) were germinated in a greenhouse at 27/25 °C day/night conditions with 60-90% relative humidity before being transplanted into larger pots 3 weeks after sowing. Plants were grown in the winter under a 12 h/12 h light/dark photoperiod, with supplemental lighting activating whenever natural light conditions dropped below approximately 500 μmol m⁻² s⁻¹. At early afternoon 56 d after sowing

2940 | Koley et al.

(a few weeks before flowering), samples were collected from the tip of the top expanded leaf using a metal plate freeze-clamp pre-chilled in liquid nitrogen to quench metabolism. The frozen samples were coarsely ground on a separate pre-chilled metal plate before being stored at -80 °C.

Sample extraction

Metabolites were extracted from ~25 or 100 mg (fresh weight) powdered camelina seeds or tobacco leaves, respectively, in 1200 μ l cold 7:3 (v/v) methanol: chloroform solution on a rotator at 4 °C for 2 h before adding 480 μ l chilled ddH₂O to separate the upper aqueous phase (modified from Ma et al., 2017). The aqueous phase was dried overnight in a speed vacuum concentrator and resuspended in either 50 μ l of 50% methanol with 0.2% formic acid for the camelina samples or 50 μ l of 50% methanol for the tobacco samples. The tobacco samples were then split into 2 × 24 μ l aliquots and brought up to a 30 μ l final volume in either 50% methanol (for HILIC runs) or 50% methanol with 0.2% formic acid (for ion exchange runs). All samples were passed through 0.8 μ m polyethersulfone clarifying filters (Sartorius) before analysis.

Liquid chromatography method

For chromatographic separation of central metabolites, a 3 µl sample was injected onto an Imtakt Intrada Organic Acid column (150 × 2 mm, 3 μm ; Kyoto, Japan) held at 40 °C using a Shimadzu Prominence-xR UFLC system. The mobile phase solvents were 100 mM ammonium formate in 10% ACN for A, and 1% final concentration of formic acid (v/v) in 10, 30, 50, 70, 75, 80, 85, or 90% ACN for the various B solvents tested, with 75% ACN being the optimal ACN concentration used for all plant samples. The following LC gradient was used: an initial concentration of 100% B held for 1 min, a linear ramp down to 88% B over 4 min, a hold at 88% B for 2 min, another ramp down to 84% B over 1 min, a hold at 84% B for 2 min, a ramp down to 75% B over 3 min, a ramp down to 0% B over 2 min, a hold at 0% B for 4.5 min for cleaning and column regeneration, followed by a ramp back up to 100% B over 30 s, and a final hold at 100% B for 5 min for equilibration. The total run time was 25 min, with a flow rate of 0.225 ml min⁻¹ used until the start of the final drop to 0% B when it was temporarily increased to 0.25 ml min⁻¹ during the column wash until the end of the run. The procedure has been deposited at protocols.io: dx.doi.org/10.17504/protocols.io.b3mvqk66.

For HILIC runs, 3 μ l of sample was injected onto an Agilent Technologies InfinityLab Poroshell 120 HILIC-Z column (2.1 \times 100 mm, 2.7 μ m) with an Agilent InfinityLab Poroshell 120 HILIC-Z guard column (2.1 \times 5 mm, 2.7 μ m) held at 40 °C. Mobile phase solvents and gradients were as previously described (Czajka *et al.*, 2020).

Mass spectrometry parameters

The eluants were detected on a SCIEX hybrid triple quadrupole-linear ion trap MS (i.e. QTRAP 6500) equipped with a Turbo VTM ESI source run in negative ionization mode. The ion source conditions used an ion spray voltage of $-4500\,\mathrm{V}$ and a source temperature of 450 °C, with the curtain gas set to 30 (arbitrary units) and the two ion source gases at 30 and 35, respectively. The diagnostic fragments and collision energies for each metabolite were determined via direct infusion of standards to generate a list of species for a targeted multiple reaction monitoring approach (Supplementary Table S1). All peak areas were integrated using the quantitation wizard in Analyst (v.1.6.2) software (SCIEX, Concord, Canada) and exported to Microsoft Excel for calculation.

Method validation and sensitivity

A 250 μ M mix of phosphorylated sugars, sugars, organic acids, and some amino acids in 50% methanol with 0.2% formic acid was serially diluted

2-fold in 50% methanol with 0.2% formic acid down to approximately 122 nM to prepare 12 concentrations of standards. Limits of detection (LOD) and quantitation (LOQ) for each metabolite were calculated by multiplying the standard deviation from the lowest concentration on the curve that showed a peak area change by 3 (for LOD) or 10 (for LOQ) and dividing by the slope of the standard curve (Nam *et al.*, 2020). A 62.5 μ M concentration of standard mix was injected 12 times on the same day and five times on different days representing different batch runs to determine intraday and interday precisions (i.e. relative standard deviation), which are indications of the repeatability and within-laboratory reproducibility of the method. Relative response factors were calculated based on the percentage of the peak area of a specific metabolite relative to the metabolite with the highest peak area, in this case UDP-glucose (UDPG), at 62.5 μ M concentration for each. The sample matrix effect for a phosphorylated sugar was determined by the following formula:

Matrix effect (%) =
$$\frac{C - (A - B)}{C} \times 100$$

Where *A* is the peak area of an analyte in a biological tobacco sample that has been spiked with 150 pmol of its standard, *B* is the peak area of that analyte in the same biological sample without addition of the standard, and *C* is the peak area of 150 pmol of the analyte standard alone (Zhou *et al.*, 2017). The precision and accuracy for the isotopic analysis were calculated from the injections of 10 unlabeled biological seed samples collected from camelina plants and compared with theoretical calculation of natural ¹³C abundance levels in metabolites using IsoCor (Millard *et al.*, 2012). Isotopologue distribution of a metabolite was calculated as the percentage of corrected abundance for each isotopologue as a fraction of the total abundances for all possible isotopologues present in the metabolite.

Results and discussion

Development of a LC method for efficient analysis of polar central carbon metabolites in the negative ionization mode of ESI-MS

Traditional anion-exchange columns are polymer-based and incompatible with buffers containing a high percentage of organic solvents; however, the hybrid column used in this study is silica-based similar to many HILIC columns. The use of buffers with a high organic component during the start of runs allows for the retention of metabolites with higher isoelectric points such as sugars that would otherwise elute in the void volume. Thus, the HILIC properties of the column can be utilized for aqueous normal phase chromatography via polarity to alter the elution of compounds in combination with the ionexchange ligand to retain negatively charged acidic analytes that are subsequently eluted by increasing ionic strength in the mobile phase. The multi-modal properties of the column were therefore explored to improve the chromatography of polar compounds in central carbon metabolism. Instead of using conventional MS-incompatible salts (potassium hydroxide) for ion-exchange, a high concentration of ammonium formate was used for gradually increasing the ionic strength of the mobile phase to elute metabolites of interest and to regenerate the column by removing tightly bound molecules. Additionally, the inclusion of 1% formic acid in the solvent B (starting mobile phase) improved ionization and created an acidic environment early in the run that promoted electrostatic interactions between the ion exchange ligand and the analytes.

A 25 min-long LC method was developed for the efficient separation of phosphorylated sugars, sugars, organic acids, and certain free amino acids on the column that were detected in the negative ionization mode of ESI-MS. A low concentration (10%) organic solvent in both buffers has previously been used to measure polar analytes in this column (Watanabe et al., 2021); however, retention of sugars and separation of phosphorylated sugar isomers were not achievable in these conditions. A wide range (10, 30, 50, 70, and 90%) of acetonitrile (ACN) in the starting buffer was tested as the first step of optimization in this study. Increasing the organic phase in solvent B resulted in greater peak sensitivities and signal-to-noise ratios (Fig. 1). While disaccharides and monosaccharides were not retained in the column using 10% ACN in the mobile phase, increasing the organic phase led to retention of sugars and their elution via increasing aqueous phase, resembling the elution in a typical HILIC column by altering polarity of the mobile phase. An ACN concentration of 70% yielded 10-47% greater peak intensities of most metabolites compared with their peaks using the traditional 10% organic phase concentration. As further ACN increases caused reductions in peak

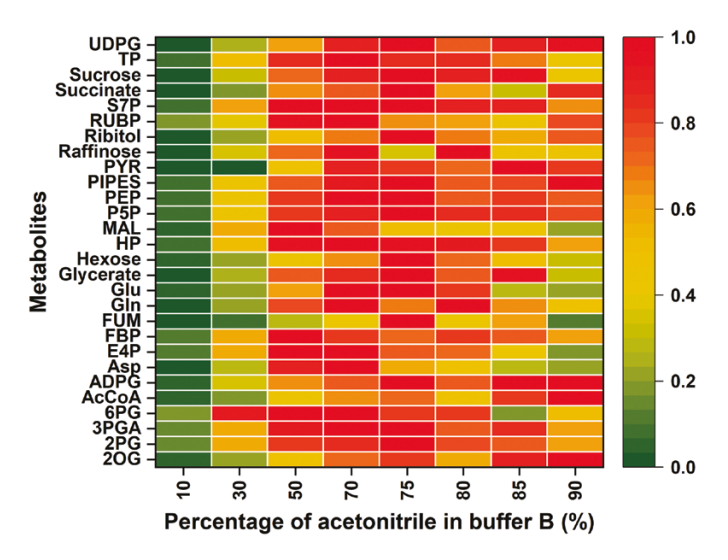


Fig. 1. Optimization of solvent B conditions to retain sugars and obtain higher sensitivity of other metabolites. A value of 1 on the scale bar denotes the highest peak area of a specific metabolites obtained from the different solvent B conditions, with lower values being relative to this highest peak area. The results are based on the mean value of three technical replicates of a 62.5 µM concentration standard mixture. 20G, α-ketoglutarate; 2PG, 2-phosphoglycolate; 3PGA, 3-phosphoglycerate; 6PG, 6-phosphogluconate; AcCoA, acetyl-CoA; ADPG, adenosine diphosphate glucose; Asp, aspartate; E4P, erythrose 4-phosphate; FBP, fructose 1,6-bisphosphate; FUM, fumarate; Gln, glutamine; Glu, glutamate; HP, hexose phosphates; MAL, malate; OAA, oxaloacetate; P5P, pentose 5-phosphate; PEP, phosphoenolpyruvate; PYR, pyruvate; RUBP, ribulose 1,5-bisphosphate; S7P, sedoheptulose 7-phosphate; TP, triose phosphates; UDPG, uridine diphosphate glucose.

intensities, a narrower range between 70 and 90% (i.e. 75, 80, and 85%) ACN concentration in B was examined for further optimization. Optimal sensitivity that captured the best peak intensities for a wide range of central metabolites utilized 75% ACN starting conditions.

Ion exchange methods typically require long run times for good separation of isomers. As the IEC-HILIC hybrid column is primarily designed for detecting organic acids, citrate and isocitrate organic acid isomers were consistently separated in all buffer conditions (see Supplementary Fig. S1); however, phosphorylated sugars were not separated using the traditional 10% ACN starting condition (Fig. 2). We observed that using a higher organic fraction in the starting solvent led to better separation of isomeric peaks without requiring an increased run time. This improved separation was potentially the combined effect of HILIC and ion exchange ligands as both the polarity and the ionic strength of the mobile phase were gradually increased during the course of a chromatographic run. Using a starting ACN concentration of 75% yielded sufficient peak separation of triose phosphates (GAP versus DHAP and 3PGA versus 2PGA), pentose phosphates (ribose 5-phosphate versus ribulose 5-phosphate), and hexose phosphates (G6P versus G1P). Increasing the ACN concentration past 75% further improved peak separation but at the expense of peak intensity and shape. Thus, a starting buffer condition of 75% ACN was judged to be optimal overall for central carbon metabolites. If further separation of multiple isomers is required, higher ACN concentrations can be utilized. For example, a 90% ACN concentration within an altered LC gradient can separate three different hexose phosphates (fructose 6-phosphate, galactose 1-phosphate and galactose 6-phosphate) (Supplementary Fig. S2) that contribute to oligosaccharides and cell wall metabolism (ElSayed et al., 2014; Gangl and Tenhaken, 2016; Althammer et al., 2020; Kambhampati et al., 2021).

Validation of the method for metabolite quantification

The sensitivity of the method to quantify low concentrations of analytes was verified by calculating the LOD and LOQ for all metabolites. The lowest analyte concentrations distinguishable from the blank and background noise ranged from femtomole to low picomole levels. Sensitive detection of various phosphorylated sugars that are intermediates of the Calvin-Benson cycle and glycolysis was observed with LOD values ranging from 250 fmol to 1.31 pmol (Table 1). Most of the organic and amino acids were also detected at similar ranges. The nucleotide sugars ADP-glucose and UDPG were found to have low LOD values of 308 and 181 fmol, respectively, while the LOD values for disaccharides and monosaccharides were limited to 4.72 and 10.95 pmol, respectively. Two internal standards (ribitol and PIPES) that are commonly used in aqueous phase extractions of polar metabolites were used in this study. The correlation coefficients of linear regression for three replicates of 12 different analyte concentrations ranging from 0.37 to 750 pmol were generally around 0.98.

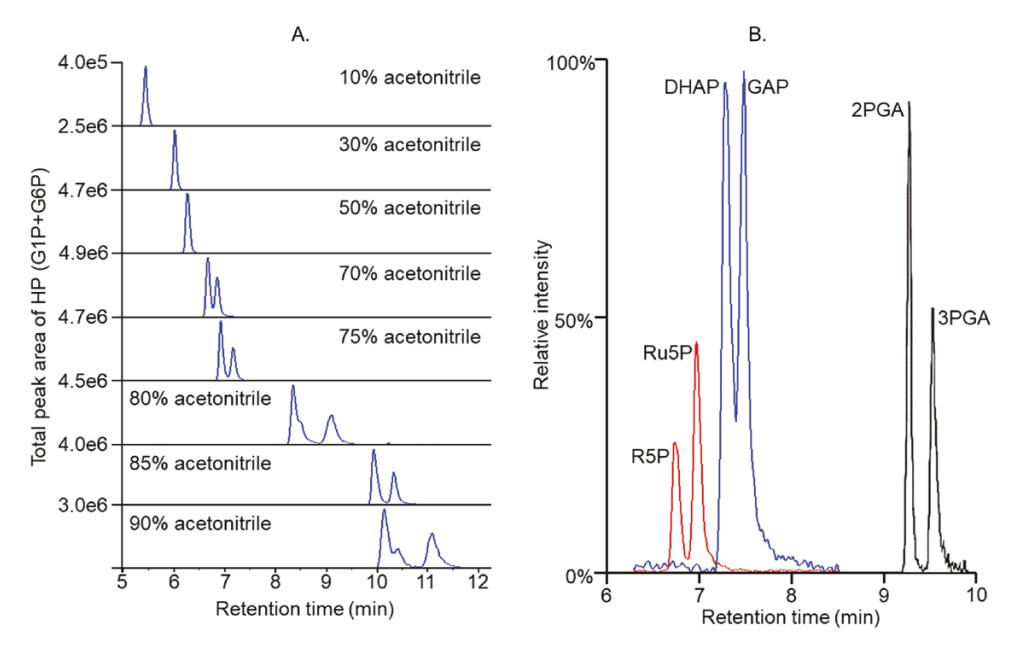


Fig. 2. Separation of phosphorylated sugar isomers. (A) Extracted ion chromatograms of the hexose phosphates glucose 1-phosphate (G1P) and glucose 6-phosphate (G6P) using different concentrations of acetonitrile in solvent B. The appearance of an additional peak at 90% acetonitrile may suggest peak splitting of G1P, an additional hexose phosphate form, or impurity in the original standard that was not resolved in lower acetonitrile concentrations. For comparison purposes, the peak areas represent the integration of all peaks. (B) Extracted ion chromatograms of the pentose phosphates ribose 5-phosphate (R5P) and ribulose 5-phosphate (Ru5P), the triose phosphates dihydroxyacetone phosphate (DHAP) and glyceraldehyde phosphate (GAP), and 2-phosphoglyceric acid (2PGA) and 3-phosphoglyceric acid (3PGA) with 75% acetonitrile in solvent B.

The calibration analysis demonstrated linearity over a wide range of concentrations (Supplementary Fig. S3), indicating a reliable quantitative relationship between metabolite levels and mass spectrometry detection using current chromatographic conditions. To check the repeatability and within-laboratory reproducibility of the method, a 62.5 µM standard mixture was injected repeatedly throughout a day and across separate batches run over a more significant period (i.e. days to months). The resulting intraday and interday coefficients of variation for most of the metabolites were less than the 15% standard value of the Food and Drug Administration (FDA) (U.S. Food and Drug Administration, 2018), demonstrating the measurement precision of the method; however, some higher variation may also represent degradation of the standard due to repeated freeze—thaw cycles or keeping the standard mix for extended periods in the autosampler.

Efficiency of the method over an alternative chromatographic approach on high lipid-producing tobacco leaf samples

Plant leaves have varied concentrations of primary metabolites, with phosphorylated sugars present at lower concentrations than sugars and organic acids. The phosphorylated sugars, however, are important intermediates comprising the CBC that describes photosynthetic metabolism in leaves, with the rapid rate of photosynthesis relative to other metabolism ensuring that these phosphorylated sugars do not accumulate to high levels and are correspondingly very sensitive to environmental

effects such as shading. It is therefore essential to be able to measure their peaks in the same method as organic acids and sugars to accurately capture foliar autotrophic metabolism. The suitability of the current method for evaluating foliar metabolism was assessed by analysing central carbon metabolites in photosynthetically competent tobacco leaf samples. To understand the efficiency of the method, leaf extracts were also run with a comparable HILIC-based method as referenced in 'Materials and methods'. Most of the phosphorylated sugars showed better peak area than their corresponding HILIC peaks when run with the hybrid column (Fig. 3). Hexose phosphates, sedoheptulose 7-phosphate, and phosphoenolpyruvate had 2to 5-fold larger peak areas on the hybrid column, while 3PGA, fructose bisphosphate, 6-phosphogluconate, triose phosphates, and pentose 5-phosphates all had greater than 5-fold increase in peak areas. The peak intensities of photorespiratory intermediates such as 2-phosphoglycolate and glyoxylate were present at low levels on the hybrid column; however, the current approach can detect these peaks sensitively due to reduced background while the peaks were frequently indistinguishable from noise using the HILIC column. Signature metabolites of the Calvin-Benson cycle such as the ribulose 1,5-bisphosphate (RUBP) substrate and 3PGA product of Rubisco and 2PGA, which provides information about glycolysis, do not give consistent peaks on the HILIC column. These key compounds showed significantly improved peak shapes and increased areas on the hybrid column (Supplementary Fig. S4). Peaks for some sugars, organic acids, and amino acids were reduced in comparison

Table 1. Performance validation of 27 analytes for quantitative analysis

Metabolites	Relative response factor (%)	Precision (RSD%)		LOD (pmol)	LOQ (pmol)	Correlation coefficient (R2)
		Intraday	Interday			
20G	4	10	13	1.25	4.16	0.9973
2PG	7	6	6	0.63	2.09	0.9928
2PGA	6	3	10	0.47	1.56	0.995
3PGA	3	6	5	0.80	2.66	0.9716
6PG	2	9	12	1.30	4.35	0.9832
AcCoA	4	31	15	3.73	12.42	0.9354
ADPG	98	7	9	0.31	1.03	0.9639
ASP	9	11	10	0.36	1.19	0.9658
DHAP	3	3	14	0.61	2.03	0.995
E4P	1	3	17	0.78	2.59	0.9921
FBP	13	5	9	0.37	1.25	0.9764
FUM	1	16	14	4.93	16.43	0.943
G1P	13	6	13	0.31	1.03	0.978
G6P	28	9	12	0.15	0.51	0.9786
GAP	2	5	17	1.31	4.37	0.9913
Gln	5	9	8	0.78	2.59	0.9655
Glu	13	9	18	0.59	1.98	0.9723
Glycerate	4	15	7	2.09	6.96	0.9519
Hexose	2	22	19	10.95	36.51	0.9306
MAL	2	8	11	1.80	6.01	0.9828
Ru5P	11	3	17	0.33	1.09	0.9909
PEP	6	8	13	0.61	2.02	0.9986
RUBP	4	8	24	0.25	0.84	0.9931
S7P	13	6	18	0.30	1.01	0.9864
Succinate	13	19	8	0.71	2.36	0.9444
Sucrose	39	4	8	4.72	15.74	0.957
UDPG	100	5	13	0.18	0.60	0.9662
PIPES*	75	4	15	0.17	0.58	0.9652
Ribitol*	2	12	11	0.39	1.31	0.9374

Relative response factors (relative to the metabolite with the highest peak area) and intraday precision were calculated from 12 injections of a 62.5 µM standard mixture while interday precision was calculated from five injections of the same standard mixture, as described in 'Materials and methods'. For other parameters, three injections of a serially diluted standard mixture ranging from 0.12 to 250 µM were used to determine the calibration curves for calculating LOD, LOQ, and correlation coefficients using the lowest concentration that still showed a peak area change. Asterisks (*) mark analytes used as internal standards in plant sample extraction. Relative standard deviation (RSD) %=(SD×100)/mean. 2OG, α-ketoglutarate; 2PG, 2-phosphoglycolate; 2PGA, 2-phosphoglycerate; 3PGA, 3-phosphoglycerate; 6PG, 6-phosphogluconate; AcCoA, acetyl-CoA; ADPG, adenosine diphosphate glucose; Asp, aspartate; DHAP, dihydroxyacetone phosphate; E4P, erythrose 4-phosphate; FBP, fructose 1,6-bisphosphate; FUM, fumarate; G1P, glucose 1-phosphate; G6P, glucose 6-phosphate; GAP, glyceraldehyde phosphate; Gln, glutamine; Glu, glutamate; MAL, malate; PEP, phosphoenolpyruvate; Ru5P, ribulose 5-phosphate; RUBP, ribulose 1,5-bisphosphate; S7P, sedoheptulose 7-phosphate; UDPG, uridine diphosphate glucose.

with the HILIC column (Fig. 3), though these metabolites tend to be abundant in most plant tissues and therefore not problematic. Thus, the use of HILIC methods may be preferable for sugar and amino/organic acid studies, but the current method is beneficial for studies of autotrophic tissues such as leaves where analysis of phosphorylated sugars is of great importance.

The difference in peak area of phosphorylated sugar standards between the run on two columns showed less variation compared with the value obtained from biological samples (Table 2). For example, fructose 1,6-bisphosphate and RUBP standards had approximately 2.5-fold smaller peak intensities on the hybrid column relative to the HILIC; however, the same compounds had larger peak areas within biological samples. This implies that the differences are likely due to increased signal to noise ratios and decreased suppression of ion

signals in the sample during the elution of phosphorylated sugars from the hybrid column. Background noise due to the mobile phase (or from medronic acid addition in the HILIC method) that can also reduce ion signal during elution of these analytes was low for the hybrid column (Supplementary Fig. S4). Further, the effect of sample matrix competes with analytes for ionizing charges (Matuszewski et al., 2003; Furey et al., 2013; Panuwet et al., 2016; Zhou et al., 2017) and may be chromatographically resolved with the hybrid system. To elucidate the effect of matrix on metabolites within the hybrid column, a mixture of standards was spiked into extracted biological samples and compared with runs of the standards at the same concentration as described by Zhou et al. (2017). The amount of ion suppression was less than 20% for all phosphorylated sugars (Fig. 4), confirming a reduced matrix

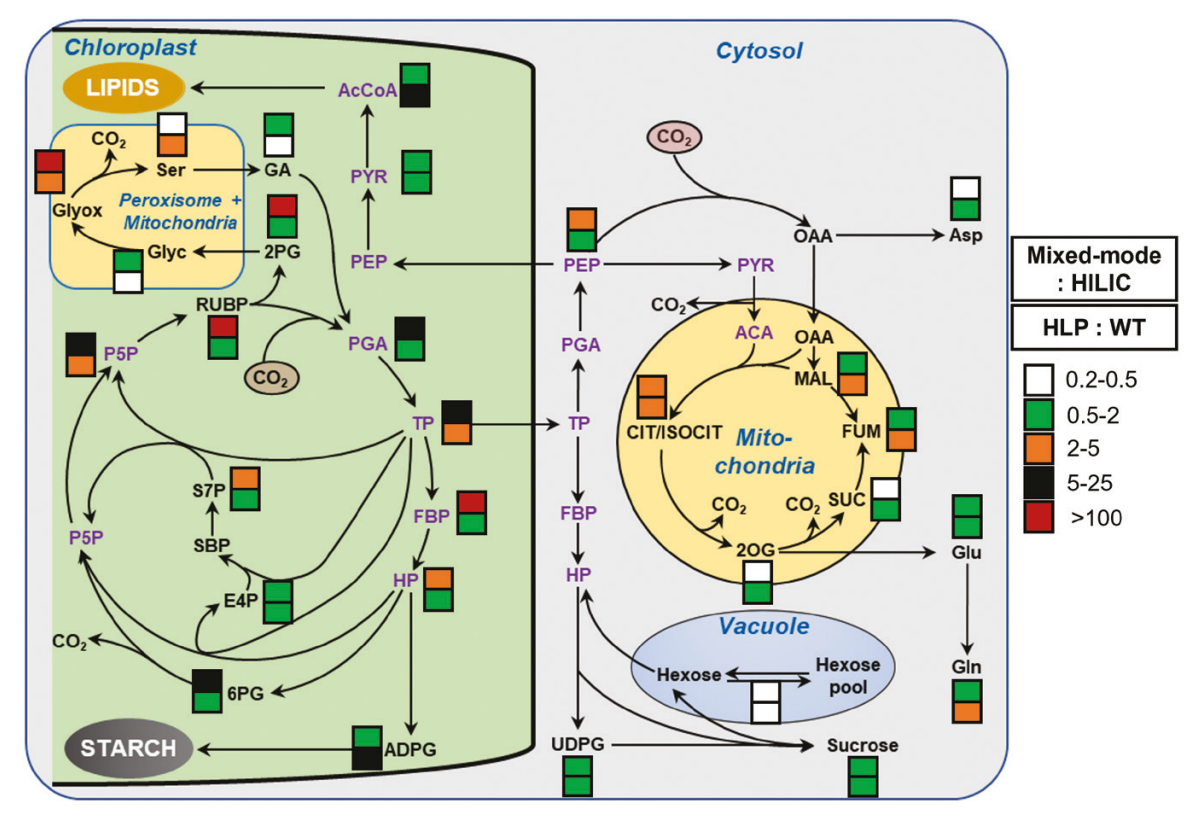


Fig. 3. Comparison of mixed-mode and HILIC chromatography using high lipid-producing (HLP) and wild-type (WT) tobacco leaves. The central metabolism model of a leaf was modified from previous studies (Ma *et al.*, 2014; Vanhercke *et al.*, 2017; Xu *et al.*, 2021; Chu *et al.*, 2022). The same sample was injected three times for both mixed-mode and HILIC chromatography. The upper box demonstrates the ratio of mixed-mode to HILIC peak areas for injections from the identical sample while the lower box demonstrates the ratio of HLP to WT sample peak areas using the mixed-mode column. Compound names in purple are metabolites found in multiple organellar locations with data shown at only one location. The results are presented as the mean value of three technical replicates. The identical biological sample with same dilution using sample buffer was injected in mixed-mode and HILIC run. 2OG, α-ketoglutarate; 2PG, 2-phosphoglycolate; 6PG, 6-phosphogluconate; AcCoA, acetyl-CoA; ADPG, adenosine diphosphate glucose; Asp, aspartate; E4P, erythrose 4-phosphate; FBP, fructose 1,6-bisphosphate; FUM, fumarate; GA, glycerate; GIn, glutamine; Glu, glutamate; Glyc, glycolate; Glyox, glyoxylate; HP, hexose phosphates; MAL, malate; OAA, oxaloacetate; P5P, pentose 5-phosphate; PEP, phosphoenolpyruvate; PGA, phosphoglyceric acid; PYR, pyruvate; RUBP, ribulose 1,5-bisphosphate; S7P, sedoheptulose 7-phosphate; SBP, sedoheptulose bisphosphate; Ser, serine; SUC, succinate; TP, triose phosphates; UDPG, uridine diphosphate glucose.

Table 2. Performance of the hybrid column for a standard mixture and a biological sample compared with a HILIC method

Metabolites	Mixed-mode to HILIC ratio			
	Standard mixture	Biological sample		
2PG	1.9	NA		
2PGA	1.8	NA		
3PGA	1.2	16.6		
6PG	1.7	8.4		
DHAP	1.7	9.3		
E4P	3.7	0.8		
FBP	0.4	105.3		
G6P	1	3.6		
Ru5P	1.6	18.6		
PEP	1.4	2.3		
RUBP	0.4	NA		
S7P	1.8	2.5		

A 50 µM standard mixture and a high lipid-producing tobacco leaf sample were run on both columns. The ratios of peak areas from the hybrid method versus a HILIC method are presented. NA denotes that the ratio was not available as the peak was not clearly detectable from noise on the HILIC column though a significant peak was found on the hybrid column. 2PG, 2-phosphoglycolate; 2PGA, 2-phosphoglycerate; 3PGA, 3-phosphoglycerate; 6PG, 6-phosphogluconate; DHAP, dihydroxyacetone phosphate; E4P, erythrose 4-phosphate; FBP, fructose 1,6-bisphosphate; G6P, glucose 6-phosphate; PEP, phosphoenolpyruvate; Ru5P, ribulose 5-phosphate; RUBP, ribulose 1,5-bisphosphate; S7P, sedoheptulose 7-phosphate.

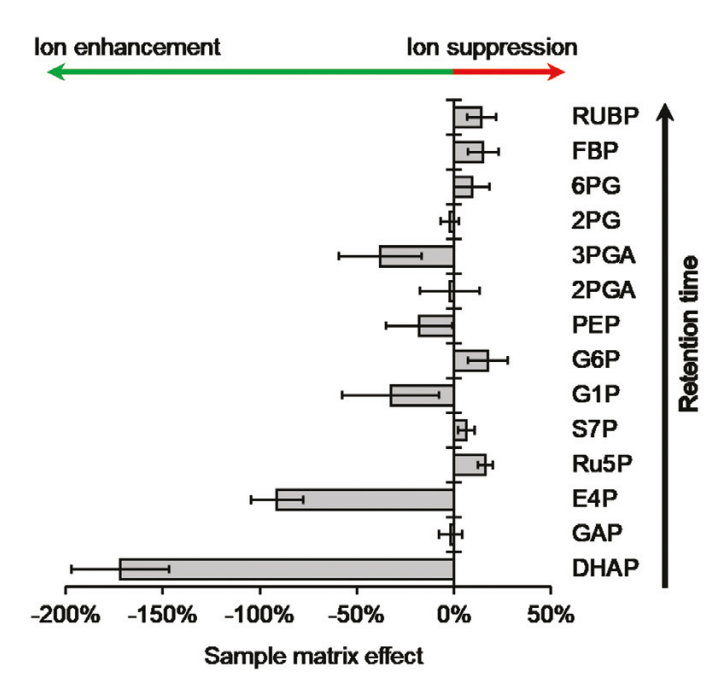


Fig. 4. Sample matrix effect on phosphorylated sugars using the hybrid column. The matrix effect was calculated based on the area of an analyte standard added to an extracted tobacco sample compared with the pure standard mixture. A 50 µM final concentration of standard mixture was used. Metabolites are presented in ascending order of retention time. A positive matrix effect denotes an ion suppression occurs, and a negative matrix effect denotes an ion enhancement occurs for a specific analyte. The results are presented as mean \pm SD (n=4 biological replicates). 2PG, 2-phosphoglycolate; 2PGA, 2-phosphoglycerate; 3PGA, 3-phosphoglycerate; 6PG, 6-phosphogluconate; DHAP, dihydroxyacetone phosphate; E4P, erythrose 4-phosphate; FBP, fructose 1,6-bisphosphate; G1P, glucose 1-phosphate; G6P, glucose 6-phosphate; GAP, glyceraldehyde phosphate; PEP, phosphoenolpyruvate; Ru5P, ribulose 5-phosphate; RUBP, ribulose 1,5-bisphosphate; S7P, sedoheptulose 7-phosphate.

interference with peaks of these metabolites. Reduced ion suppression has been reported using a mixed-mode column that showed comparatively less column-bleed than a singlemode column (Lien et al., 2009; Walter et al., 2021). Unlike many other columns, the hybrid column used in the current study is metal-free, which facilitates less adsorption and loss of analytes, especially phosphorylated compounds (Zhao et al., 2009; Tian et al., 2010). Further, at the beginning of a chromatographic run, anion exchange columns elute ions with higher isoelectric points than the pH of starting buffer, resulting in reduced competition for ions with metabolites that elute later. The significant ion enhancement observed for phosphoenolpyruvate, G1P, erythrose 4-phosphate, and DHAP, was not specific to retention time windows and therefore not likely specific to a solvent condition.

Central carbon metabolite profiles were compared between wild-type and HLP tobacco leaves (first genetically described in Vanhercke et al., 2017). These HLP leaves can accumulate triacylglycerol to around 30% of their dry weight, a

level comparable to oilseeds, versus the minor triacylglycerol amounts (<1% dry weight) normally found in plant leaves. Acetyl-CoA, an important precursor in fatty acid biosynthesis, was 5-fold greater in the HLP leaves and more sensitively detected on the hybrid column (Fig. 3). As kits for acetyl-CoA measurement can be inconsistent, the accurate measurement of this metabolite is of sustained importance to lipid metabolism studies. Large differences in the levels of certain amino acids. organic acids, and phosphorylated sugars were also observed for the HLP line, suggestive of the major metabolic changes that occurred in the oil-accumulating leaves.

Application of the method for isotopic analysis using oilseed samples

For flux measurements, the precision and accuracy of the isotopologue distribution of metabolites are important (Antoniewicz et al., 2006; McCloskey et al., 2016; Jaiswal et al., 2018). The accuracy (deviation of measured values compared with theoretical natural abundance) and precision of this method were assessed by analysing both ^{12}C (M_0) and ^{13}C (M_1) isotopologues of central carbon metabolites from camelina seeds 15 d after flowering (mid-maturity) relative to theoretically expected values from natural abundance. The coefficient of variation of the ratio of M_1 to M_0 for 10 biological samples ranged from 1% to 21% (Table 3), with most metabolites under the 15% FDA standard (U.S. Food and Drug Administration, 2018). Absolute accuracies within 1% from LC-MS data are desirable to increase confidence for flux values (Antoniewicz, 2018). The error in absolute accuracy for most metabolites was less than 1.2% while the relative accuracy varied from 84% to 106%. More significant deviation in M_1/M_0 versus the theoretical value observed for acetyl-CoA could be explained by differences in ¹³C incorporation in carbons of the CoA moiety versus the acetyl portion.

The application of this method for ¹³C-labeling experiments was further demonstrated by examining camelina embryos cultured in a medium containing [U-13C]glucose as described in Romsdahl et al. (2021) with additional multiple reaction monitoring added for labeled isotopologues of metabolites. Labeling changes in a few important central metabolites from each group of sugars, phosphorylated sugars, and organic acids are presented in Fig. 5. A typical enriching effect was observed over time, with single and minimally labeled isotopologues initially increasing and then decreasing as more labeled isotopologues became enriched with ¹³C. As [U-¹³C₆] glucose was supplied to the medium, the M_6 isotopologue of G6P, UDPG, and sucrose increased over 10 h. Label enrichment was also observed in acetyl-CoA, indicating the active supply of precursors for oil biosynthesis in camelina seed. Further validation of the method was indicated by the similar labeling patterns seen for precursor-product or network-related metabolites such as 3PGA and GAP or G6P and UDPG.

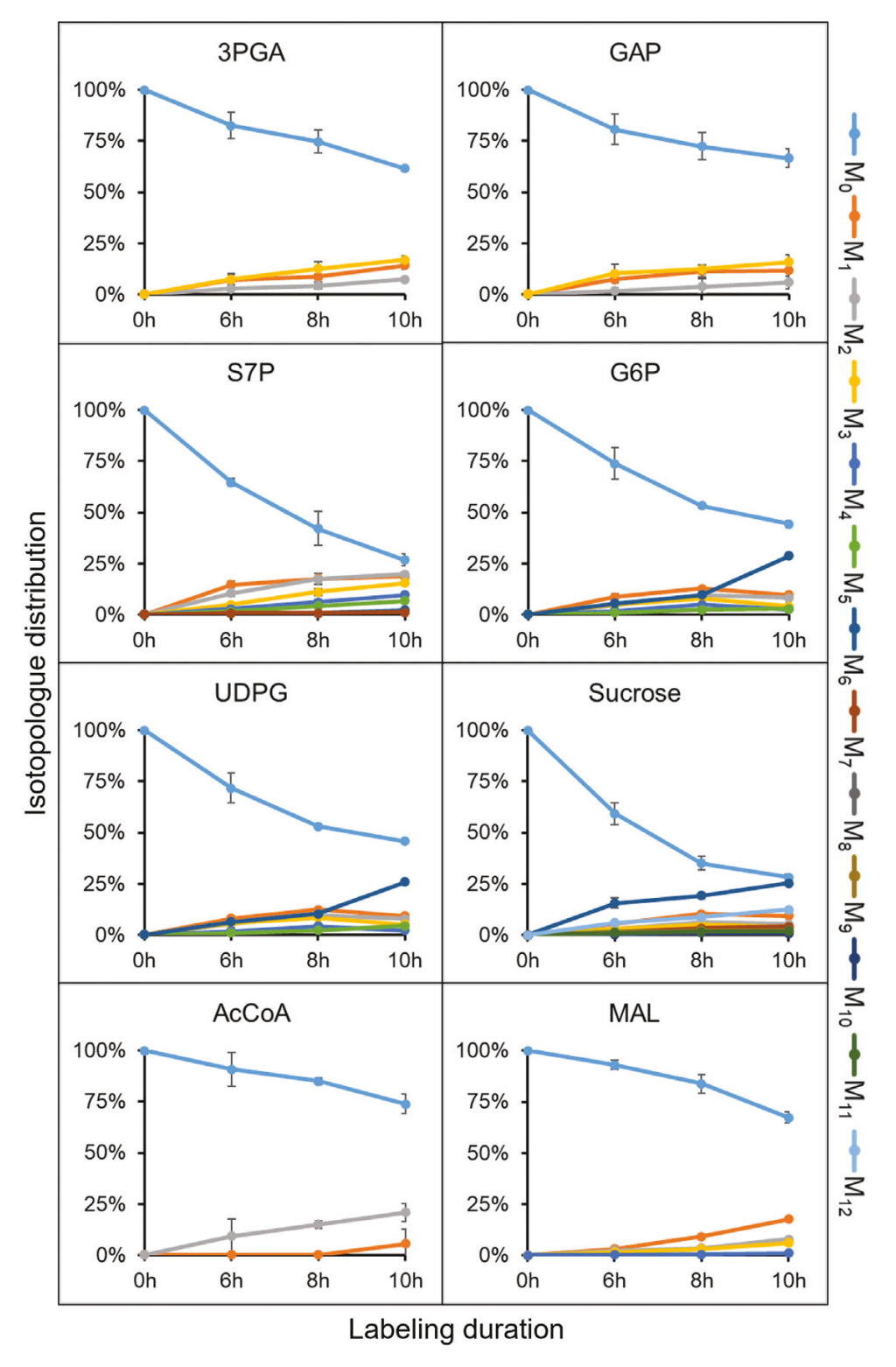


Fig. 5. Visualization of changes in 13 C-labeling phenotypes in camelina seed. Labeling kinetics of 3-phosphoglyceric acid (3PGA), glyceraldehyde phosphate (GAP), sedoheptulose 7-phosphate (S7P), glucose 6-phosphate (G6P), UDP-glucose (UDPG), sucrose, acetyl CoA (AcCoA), and malate (MAL) presented as amount of 13 C present in these metabolites over a labeling period of 6, 8, and 10 h from a source of [U- 13 C]glucose. The different labeled isotopologues are denoted as M_0 , M_1 , M_2 , etc., indicating the number of 13 C atoms present in the compound. The results are presented as mean \pm SD (n=3 biological replicates).

Table 3. Precision and accuracy of isotopologue distributions for labeling studies

Metabolites	M_1/M_0					
	Precision	Accuracy	Absolute accuracy			
20G	9%	95%	0.28%			
6PG	21%	84%	1.16%			
AcCoA	13%	56%	13.03%			
Asp	4%	97%	0.14%			
CIT	1%	96%	0.29%			
FBP	14%	88%	0.89%			
FUM	6%	106%	0.25%			
Gln	1%	100%	0.03%			
Glu	2%	98%	0.12%			
HP	11%	96%	0.27%			
MAL	1%	96%	0.17%			
P5P	12%	92%	0.50%			
PEP	17%	83%	0.60%			
PGA	10%	87%	0.49%			
RUBP	16%	94%	0.34%			
S7P	11%	98%	0.14%			
Succinate	19%	82%	0.84%			
Sucrose	2%	101%	0.08%			
TP	13%	97%	0.11%			
UDPG	3%	102%	0.10%			

The calibration was performed using 10 biological samples of 15 d after flowering camelina seed. Unlabeled (M_0) and single labeled (M_1) isotopologues comprise over 98% of the total for small molecule natural abundance profiles. The ratio of the two isotopologues were compared for biological samples relative to theoretically predicted values based on established natural abundance levels (Rosman and Taylor, 1998). Precision was assessed as the coefficient of variation of M_1/M_0 measured for each metabolite from 10 biological samples. Accuracy was based on the measured M_1/M_0 divided by the theoretical value where absolute accuracy is the absolute difference between measured and theoretical values. 2OG, a-ketoglutarate; 6PG, 6-phosphogluconate; AcCoA, acetyl-CoA; Asp, aspartate; CIT, citrate; FBP, fructose 1,6-bisphosphate; FUM, fumarate; Gln, glutamine; Glu, glutamate; HP, hexose phosphates; MAL, malate; P5P, pentose 5-phosphate; PEP, phosphoenolpyruvate; PGA, phosphoglyceric acid; RUBP, ribulose 1,5-bisphosphate; S7P, sedoheptulose 7-phosphate; TP, triose phosphates; UDPG, uridine diphosphate glucose.

Conclusion

A chromatography method combining the ion-exchange and HILIC properties of a mixed mode hybrid column was developed to accurately assess a wide range of metabolites in central carbon metabolism. The combination of aqueous normal phase chromatography with anion-exchange chromatography provided the retention and elution of sugars, phosphorylated sugars, amino acids, and organic acids with larger peak areas. Isomers of phosphorylated sugars in central metabolism have significant relevance for a detailed understanding of the subcellular metabolism in plant organs including leaves and seeds. Altering both the polarity and ionic strength of the mobile phase during the chromatographic run facilitated the separation of these key isomers without requiring a long run time. The method does not require MS-incompatible salts nor buffer additives such as ionpairing reagents that contaminate the instrument. Sensitive and reproducible peaks over several orders of magnitude of concentration were obtained with good accuracy and precision such that it will be applicable for stable isotope-labeling studies. The sensitivity of this approach for low abundance phosphorylated sugars that are signature metabolites in photosynthetic metabolism in leaf tissues was improved compared with other columns and related to limited matrix effect. Thus, the current studies provide a method for the analysis of central carbon metabolism

in photosynthetic tissues that can advance research efforts in plants by providing a more complete and accurate assessment of their low abundance and isomeric metabolic intermediates.

Supplementary data

The following supplementary data are available at *JXB* online. Fig. S1. Separation of citrate and isocitrate isomers using the Imtakt organic acid column.

Fig. S2. Separation of three hexose phosphate isomers using 90% acetonitrile in solvent B.

Fig. S3. Calibration curves of 27 metabolites plus PIPES and ribitol from a serially diluted standard mixture using the optimized LC-MS method.

Fig. S4. Detection of RUBP and PGA from a biological sample using HILIC versus hybrid column.

Table S1. Compound specific mass spectrometry parameters of analytes used in this study.

Acknowledgements

We thank Dr Xue-Rong Zhou (Commonwealth Scientific and Industrial Research Organisation (CSIRO)) for providing WT and HLP transgenic tobacco seeds; Dr Brad Evans (Proteomics and Mass Spectrometry Facility,

2948 | Koley et al.

Donald Danforth Plant Science Center) for his assistance with LC-MS instrumentation; Kevin Reilly, Kris Haines, Stephen Kraeuter, and Aileen Wok (Integrated Plant Growth Facility, Donald Danforth Plant Science Center) for their assistance with plant growth and propagation; and the U.S. Department of Agriculture (USDA) Agricultural Research Service (ARS) for further support.

Author contributions

SK and DKA conceived the research; SK and SSG performed the method optimization; KLC and SK performed the method validation, and SK performed the labeling study; SK and KLC analysed the data with the assistance of DKA and contributed to scope; SK and KLC wrote the article with the assistance of DKA and it was approved by all authors.

Conflict of interest

The authors have no conflict of interest to declare.

Funding

The authors acknowledge support for aspects of this work from National Science Foundation award (IOS-1829365), USDA-National Institute of Food and Agriculture (USDA-NIFA) (2017-67013-26156) and a subaward from the University of Illinois as part of the research project Realizing Increased Photosynthetic Efficiency that is funded by the Bill & Melinda Gates Foundation, the Foundation for Food & Agriculture Research, and the UK government's Department for International Development under Grant No. OPP1172157. KLC and SSG were supported in part by an appointment to the Research Participation Program administered by the Oak Ridge Institute for Science and Education (ORISE) through an interagency agreement between the U.S. Department of Energy (DOE), and the USDA-ARS. ORISE is managed by ORAU under DOE contract number DE-SC0014664. The QTRAP LC-MS/MS instrument which was used in the study was acquired through National Science Foundation award (DBI-1427621).

Data availability

The data supporting the findings of this study are available from the corresponding authors (SK and DKA), upon request. The liquid chromatography method is deposited at protocols.io: dx.doi.org/10.17504/protocols.io.b3mvqk66.

References

Allen DK. 2016. Quantifying plant phenotypes with isotopic labeling & metabolic flux analysis. Current Opinion in Biotechnology **37**, 45–52.

Allen DK, Libourel IG, Shachar-Hill Y. 2009. Metabolic flux analysis in plants: coping with complexity. Plant, Cell & Environment **32**, 1241–1257.

Allen DK, Young JD. 2013. Carbon and nitrogen provisions alter the metabolic flux in developing soybean embryos. Plant Physiology **161**, 1458–1475.

Allen DK, Young JD. 2020. Tracing metabolic flux through time and space with isotope labeling experiments. Current Opinion in Biotechnology **64**, 92–100.

Allwood JW, De Vos RC, Moing A, Deborde C, Erban A, Kopka J, Goodacre R, Hall RD. 2011. Plant metabolomics and its potential for

systems biology research background concepts, technology, and methodology. Methods in Enzymology **500**, 299–336.

Alonso AP, Piasecki RJ, Wang Y, LaClair RW, Shachar-Hill Y. 2010. Quantifying the labeling and the levels of plant cell wall precursors using ion chromatography tandem mass spectrometry. Plant Physiology 153, 915–924.

Althammer M, Blöchl C, Reischl R, Huber CG, Tenhaken R. 2020. Phosphoglucomutase is not the target for galactose toxicity in plants. Frontiers in Plant Science **11**, 167.

Annesley TM. 2003. Ion suppression in mass spectrometry. Clinical Chemistry **49**, 1041–1044.

Antoniewicz MR. 2013. Dynamic metabolic flux analysis—tools for probing transient states of metabolic networks. Current Opinion in Biotechnology **24**, 973–978.

Antoniewicz MR. 2018. A guide to ¹³C metabolic flux analysis for the cancer biologist. Experimental & Molecular Medicine **50**, 1–13.

Antoniewicz MR, Kelleher JK, Stephanopoulos G. 2006. Determination of confidence intervals of metabolic fluxes estimated from stable isotope measurements. Metabolic Engineering **8**, 324–337.

Arrivault S, Guenther M, Ivakov A, Feil R, Vosloh D, van Dongen JT, Sulpice R, Stitt M. 2009. Use of reverse-phase liquid chromatography, linked to tandem mass spectrometry, to profile the Calvin cycle and other metabolic intermediates in Arabidopsis rosettes at different carbon dioxide concentrations. The Plant Journal 59, 826–839.

Arrivault S, Obata T, Szecówka M, Mengin V, Guenther M, Hoehne M, Fernie AR, Stitt M. 2017. Metabolite pools and carbon flow during C_4 photosynthesis in maize: $^{13}\text{CO}_2$ labeling kinetics and cell type fractionation. Journal of Experimental Botany **68**, 283–298.

AuBuchon-Elder T, Coneva V, Goad DM, Jenkins LM, Yu Y, Allen DK, Kellogg EA. 2020. Sterile spikelets contribute to yield in sorghum and related grasses. The Plant Cell **32**, 3500–3518.

Balcke GU, Bennewitz S, Bergau N, Athmer B, Henning A, Majovsky P, Jiménez-Gómez JM, Hoehenwarter W, Tissier A. 2017. Multi-omics of tomato glandular trichomes reveals distinct features of central carbon metabolism supporting high productivity of specialized metabolites. The Plant Cell 29, 960–983.

Balcke GU, Bennewitz S, Zabel S, Tissier A. 2014. Isoprenoid and metabolite profiling of plant trichomes. In: Rodríguez-Concepción M, ed. Plant isoprenoids: Methods and protocols. Methods in Molecular Biology Vol 1153. New York: Springer, 189–202.

Bino RJ, Hall RD, Fiehn O, et al. 2004. Potential of metabolomics as a functional genomics tool. Trends in Plant Science **9**, 418–425.

Castells CB, Arias VC, Castells RC. 2002. Precolumn derivatization of reducing carbohydrates with 4-(3-methyl-5-oxo-2-pyrazolin-1-yl) benzoic acid. Study of reaction, high-performance liquid chromatographic separation and quantitative performance of method. Chromatographia **56**, 153.

Choi J, Antoniewicz MR. 2019. Tandem mass spectrometry for ¹³C metabolic flux analysis: methods and algorithms based on EMU framework. Frontiers in Microbiology **10**, 31.

Chu KL, Koley S, Jenkins LM, et al. 2022. Metabolic flux analysis of the non-transitory starch tradeoff for lipid production in mature tobacco leaves. Metabolic Engineering **69**, 231–248.

Colón AM, Sengupta N, Rhodes D, Dudareva N, Morgan J. 2010. A kinetic model describes metabolic response to perturbations and distribution of flux control in the benzenoid network of *Petunia hybrida*. The Plant Journal **62**, 64–76.

Coulier L, Bas R, Jespersen S, Verheij E, van der Werf MJ, Hankemeier T. 2006. Simultaneous quantitative analysis of metabolites using ion-pair liquid chromatography-electrospray ionization mass spectrometry. Analytical Chemistry **78**, 6573–6582.

Czajka JJ, Kambhampati S, Tang YJ, Wang Y, Allen DK. 2020. Application of stable isotope tracing to elucidate metabolic dynamics during *Yarrowia lipolytica* α -ionone fermentation. IScience **23**, 100854.

Daloso DM, Antunes WC, Pinheiro DP, Waquim JP, Araújo WL, Loureiro ME, Fernie AR, Williams TC. 2015. Tobacco guard cells fix CO_2

by both Rubisco and PEPcase while sucrose acts as a substrate during light-induced stomatal opening. Plant, Cell & Environment 38, 2353-2371.

de Jong FA, Beecher C. 2012. Addressing the current bottlenecks of metabolomics: isotopic Ratio Outlier AnalysisTM, an isotopic-labeling technique for accurate biochemical profiling. Bioanalysis 4, 2303-2314.

Dethloff F, Orf I, Kopka J. 2017. Rapid in situ ¹³C tracing of sucrose utilization in Arabidopsis sink and source leaves. Plant Methods 13, 87.

Dias DA, Hill CB, Jayasinghe NS, Atieno J, Sutton T, Roessner U. 2015. Quantitative profiling of polar primary metabolites of two chickpea cultivars with contrasting responses to salinity. Journal of Chromatography B 1000. 1-13.

Doerr A. 2017. Global metabolomics. Nature Methods 14, 32-32.

ElSayed Al, Rafudeen MS, Golldack D. 2014. Physiological aspects of raffinose family oligosaccharides in plants: protection against abiotic stress. Plant Biology 16, 1-8.

Fan TW-M, El-Amouri SS, Macedo JKA, Wang QJ, Song H, Cassel T, Lane AN. 2018. Stable isotope-resolved metabolomics shows metabolic resistance to anti-cancer selenite in 3D spheroids versus 2D cell cultures. Metabolites 8, 40.

Fan TW-M, Lorkiewicz PK, Sellers K, Moseley HN, Higashi RM, Lane AN. 2012. Stable isotope-resolved metabolomics and applications for drug development. Pharmacology & Therapeutics 133, 366-391.

Fenn JB, Mann M, Meng CK, Wong SF, Whitehouse CM. 1989. Electrospray ionization for mass spectrometry of large biomolecules. Science 246, 64-71.

Fernie AR, Geigenberger P, Stitt M. 2005. Flux an important, but neglected, component of functional genomics. Current Opinion in Plant Biology **8**. 174-182.

Fernie AR. Morgan JA. 2013. Analysis of metabolic flux using dynamic labelling and metabolic modelling. Plant, Cell & Environment 36, 1738–1750.

Fessenden M. 2016. Metabolomics: small molecules, single cells. Nature **540**, 153-155.

Fiehn O, Kopka J, Dörmann P, Altmann T, Trethewey RN, Willmitzer L. 2000. Metabolite profiling for plant functional genomics. Nature Biotechnology 18, 1157-1161.

Furey A, Moriarty M, Bane V, Kinsella B, Lehane M. 2013. lon suppression; a critical review on causes, evaluation, prevention and applications. Talanta 115, 104-122.

Gangl R, Tenhaken R. 2016. Raffinose family oligosaccharides act as galactose stores in seeds and are required for rapid germination of Arabidopsis in the dark. Frontiers in Plant Science 7, 1115.

Giavalisco P, Köhl K, Hummel J, Seiwert B, Willmitzer L. 2009. 13C isotope-labeled metabolomes allowing for improved compound annotation and relative quantification in liquid chromatography-mass spectrometrybased metabolomic research. Analytical Chemistry 81, 6546-6551.

Giavalisco P, Li Y, Matthes A, Eckhardt A, Hubberten HM, Hesse H, Segu S, Hummel J, Köhl K, Willmitzer L. 2011. Elemental formula annotation of polar and lipophilic metabolites using $^{\rm 13}{\rm C},~^{\rm 15}{\rm N}$ and $^{\rm 34}{\rm S}$ isotope labelling, in combination with high-resolution mass spectrometry. The Plant Journal 68, 364-376.

Hasunuma T. Harada K. Miyazawa S. Kondo A. Fukusaki E. Miyake C. 2010. Metabolic turnover analysis by a combination of in vivo ¹³C-labelling from ¹³CO₂ and metabolic profiling with CE-MS/MS reveals rate-limiting steps of the C₃ photosynthetic pathway in Nicotiana tabacum leaves. Journal of Experimental Botany 61, 1041-1051.

Heaton JC. McCalley DV. 2016. Some factors that can lead to poor peak shape in hydrophilic interaction chromatography, and possibilities for their remediation. Journal of Chromatography A 1427, 37-44.

Heise R, Arrivault S, Szecowka M, Tohge T, Nunes-Nesi A, Stitt M, Nikoloski Z, Fernie AR. 2014. Flux profiling of photosynthetic carbon metabolism in intact plants. Nature Protocols 9, 1803-1824.

Heux S, Bergès C, Millard P, Portais JC, Létisse F. 2017. Recent advances in high-throughput ¹³C-fluxomics. Current Opinion in Biotechnology **43**. 104-109.

Higashi RM, Fan TWM, Lorkiewicz PK, Moseley HNB, Lane AN. 2014. Stable isotope-labeled tracers for metabolic pathway elucidation by GC-MS and FT-MS. In: Raftery D, ed. Mass spectrometry in metabolomics: methods and protocols, methods in molecular biology. New York: Springer, 147–167.

Higashi T, Ogawa S. 2020. Derivatization-based sample-multiplexing for enhancing throughput in liquid chromatography/tandem mass spectrometry quantification of metabolites: an overview. Journal of Chromatography A 1634, 461679.

Hsiao JJ. Potter OG. Chu TW. Yin H. 2018. Improved LC/MS methods for the analysis of metal-sensitive analytes using medronic acid as a mobile phase additive. Analytical Chemistry 90, 9457-9464.

Huege J, Sulpice R, Gibon Y, Lisec J, Koehl K, Kopka J. 2007. GC-El-TOF-MS analysis of in vivo carbon-partitioning into soluble metabolite pools of higher plants by monitoring isotope dilution after ¹³CO₂ labelling. Phytochemistry 68, 2258-2272.

Iturrospe E, Da Silva KM, Talavera Andújar B, Cuykx M, Boeckmans J, Vanhaecke T, Covaci A, van Nuijs ALN. 2021. An exploratory approach for an oriented development of an untargeted hydrophilic interaction liquid chromatography-mass spectrometry platform for polar metabolites in biological matrices. Journal of Chromatography A 1637, 461807.

Jaiswal D, Prasannan CB, Hendry JI, Wangikar PP. 2018. SWATH tandem mass spectrometry workflow for quantification of mass isotopologue distribution of intracellular metabolites and fragments labeled with isotopic ¹³C carbon. Analytical Chemistry **90**, 6486–6493.

Jandera P. 2011. Stationary and mobile phases in hydrophilic interaction chromatography: a review. Analytica Chimica Acta 692, 1-25.

Johnson JR. Karlsson D. Dalene M. Skarping G. 2010. Determination of aromatic amines in aqueous extracts of polyurethane foam using hydrophilic interaction liquid chromatography and mass spectrometry. Analytica Chimica Acta 678, 117-123.

Jorge TF, Rodrigues JA, Caldana C, Schmidt R, van Dongen JT, Thomas-Oates J, António C. 2016. Mass spectrometry-based plant metabolomics: metabolite responses to abiotic stress. Mass Spectrometry Reviews 35, 620-649.

Kambhampati S, Aznar-Moreno JA, Bailey SR, Arp JJ, Chu KL, Bilyeu KD. Durrett TP. Allen DK. 2021. Temporal changes in metabolism late in seed development affect biomass composition. Plant Physiology 186,

Kebarle P, Tang L. 1993. From ions in solution to ions in the gas phase - the mechanism of electrospray mass spectrometry. Analytical Chemistry 65, 972A-986A.

Kiefer P. Nicolas C. Letisse F. Portais JC. 2007. Determination of carbon labeling distribution of intracellular metabolites from single fragment ions by ion chromatography tandem mass spectrometry. Analytical Biochemistry **360**. 182-188.

Kim HK, Choi YH, Verpoorte R. 2010. NMR-based metabolomic analysis of plants. Nature Protocols 5, 536-549.

Kim HK, Choi YH, Verpoorte R. 2011. NMR-based plant metabolomics: where do we stand, where do we go? Trends in Biotechnology 29,

Kim T, Dreher K, Nilo-Poyanco R, et al. 2015. Patterns of metabolite changes identified from large-scale gene perturbations in Arabidopsis using a genome-scale metabolic network. Plant Physiology 167, 1685-1698.

Koley S, Raorane ML, Junker BH. 2019. Shoot tip culture: a step towards ¹³C metabolite flux analysis of sink leaf metabolism. Plant Methods **15**. 48.

Kvitvang HF, Kristiansen KA, Bruheim P. 2014. Assessment of capillary anion exchange ion chromatography tandem mass spectrometry for the quantitative profiling of the phosphometabolome and organic acids in biological extracts. Journal of Chromatography A 1370, 70-79.

Kwon H, Kim J. 1993. Determination of monosaccharides in glycoproteins by reverse-phase high-performance liquid chromatography. Analytical Biochemistry 215, 243-252.

Lien GW. Chen CY. Wang GS. 2009. Comparison of electrospray ionization, atmospheric pressure chemical ionization and atmospheric pressure

- photoionization for determining estrogenic chemicals in water by liquid chromatography tandem mass spectrometry with chemical derivatizations. Journal of Chromatography A **1216**, 956–966.
- **Liu X, Enright M, Barry CS, Jones AD.** 2017. Profiling, isolation and structure elucidation of specialized acylsucrose metabolites accumulating in trichomes of *Petunia* species. Metabolomics **13**, 85.
- **Ma F, Jazmin LJ, Young JD, Allen DK.** 2014. Isotopically nonstationary ¹³C flux analysis of changes in *Arabidopsis thaliana* leaf metabolism due to high light acclimation. Proceedings of the National Academy of Sciences, USA **111**, 16967–16972.
- **Ma F, Jazmin LJ, Young JD, Allen DK.** 2017. Isotopically nonstationary metabolic flux analysis (INST-MFA) of photosynthesis and photorespiration in plants. In: Fernie AR, Bauwe H, Weber APM, eds. Photorespiration: methods and protocols, methods in molecular biology. New York: Springer, 167–194
- Mansfeld BN, Colle M, Kang Y, Jones AD, Grumet R. 2017. Transcriptomic and metabolomic analyses of cucumber fruit peels reveal a developmental increase in terpenoid glycosides associated with age-related resistance to *Phytophthora capsici*. Horticulture Research 4, 17022.
- **Masakapalli SK, Ratcliffe RG, Williams TCR.** 2014a. Quantification of ¹³C enrichments and isotopomer abundances for metabolic flux analysis using 1D NMR spectroscopy. In: Dieuaide-Noubhani M, Alonso AP, eds. Plant metabolic flux analysis: methods and protocols, methods in molecular biology. Totowa, NJ: Humana Press, 73–86.
- Masakapalli SK, Ritala A, Dong L, van der Krol AR, Oksman-Caldentey KM, Ratcliffe RG, Sweetlove LJ. 2014b. Metabolic flux phenotype of tobacco hairy roots engineered for increased geraniol production. Phytochemistry 99, 73–85.
- **Matuszewski BK, Constanzer ML, Chavez-Eng CM.** 2003. Strategies for the assessment of matrix effect in quantitative bioanalytical methods based on HPLC-MS/MS. Analytical Chemistry **75**, 3019–3030.
- **McCloskey D, Young JD, Xu S, Palsson BO, Feist AM.** 2016. MID Max: LC-MS/MS method for measuring the precursor and product mass isotopomer distributions of metabolic intermediates and cofactors for metabolic flux analysis applications. Analytical Chemistry **88**, 1362–1370.
- Millard P, Enjalbert B, Uttenweiler-Joseph S, Portais JC, Létisse F. 2021. Control and regulation of acetate overflow in *Escherichia coli*. eLife **10**. e63661.
- Millard P, Letisse F, Sokol S, Portais JC. 2012. IsoCor: correcting MS data in isotope labeling experiments. Bioinformatics 28, 1294–1296.
- Milne SB, Mathews TP, Myers DS, Ivanova PT, Brown HA. 2013. Sum of the parts: mass spectrometry-based metabolomics. Biochemistry **52**, 3829–3840.
- **Myint KT, Uehara T, Aoshima K, Oda Y.** 2009. Polar anionic metabolome analysis by nano-LC/MS with a metal chelating agent. Analytical Chemistry **81**, 7766–7772.
- Nam JW, Jenkins LM, Li J, Evans BS, Jaworski JG, Allen DK. 2020. A general method for quantification and discovery of acyl groups attached to acyl carrier proteins in fatty acid metabolism using LC-MS/MS. The Plant Cell 32, 820–832.
- **Nöh K, Wiechert W.** 2006. Experimental design principles for isotopically instationary ¹³C labeling experiments. Biotechnology and Bioengineering **94**, 234–251.
- **Nordström A, Tarkowski P, Tarkowska D, Dolezal K, Astot C, Sandberg G, Moritz T.** 2004. Derivatization for LC-electrospray ionization-MS: a tool for improving reversed-phase separation and ESI responses of bases, ribosides, and intact nucleotides. Analytical Chemistry **76**, 2869–2877.
- **O'Grady J, Schwender J, Shachar-Hill Y, Morgan JA.** 2012. Metabolic cartography: experimental quantification of metabolic fluxes from isotopic labelling studies. Journal of Experimental Botany **63**, 2293–2308.
- Panuwet P, Hunter RE Jr, D'Souza PE, Chen X, Radford SA, Cohen JR, Marder ME, Kartavenka K, Ryan PB, Barr DB. 2016. Biological matrix effects in quantitative tandem mass spectrometry-based analytical methods: advancing biomonitoring. Critical Reviews in Analytical Chemistry 46, 93–105.
- Petucci C, Zelenin A, Culver JA, Gabriel M, Kirkbride K, Christison TT, Gardell SJ. 2016. Use of ion chromatography/mass spectrometry for

- targeted metabolite profiling of polar organic acids. Analytical Chemistry 88, 11799–11803.
- **Quanbeck SM, Brachova L, Campbell AA, et al.** 2012. Metabolomics as a hypothesis-generating functional genomics tool for the annotation of *Arabidopsis thaliana* genes of "unknown function". Frontiers in Plant Science **3**, 15.
- **Rende U, Niittylä T, Moritz T.** 2019. Two-step derivatization for determination of sugar phosphates in plants by combined reversed phase chromatography/tandem mass spectrometry. Plant Methods **15**, 127.
- Roessner U, Luedemann A, Brust D, Fiehn O, Linke T, Willmitzer L, Fernie A. 2001. Metabolic profiling allows comprehensive phenotyping of genetically or environmentally modified plant systems. The Plant Cell 13, 11–29.
- **Roessner-Tunali U, Liu J, Leisse A, Balbo I, Perez-Melis A, Willmitzer L, Fernie AR.** 2004. Kinetics of labelling of organic and amino acids in potato tubers by gas chromatography-mass spectrometry following incubation in ¹³C labelled isotopes. The Plant Journal **39**, 668–679.
- Romsdahl TB, Kambhampati S, Koley S, Yadav UP, Alonso AP, Allen DK, Chapman KD, 2021. Analyzing mass spectrometry imaging data of ¹³C-labeled phospholipids in *Camelina sativa* and *Thlaspi arvense* (pennycress) embryos. Metabolites **11**, 148.
- **Rosman KJR, Taylor PDP.** 1998. Isotopic compositions of the elements 1997. Journal of Physical and Chemical Reference Data **27**, 1275–1287.
- Sarvin B, Lagziel S, Sarvin N, Mukha D, Kumar P, Aizenshtein E, Shlomi T. 2020. Fast and sensitive flow-injection mass spectrometry metabolomics by analyzing sample-specific ion distributions. Nature Communications 11. 3186.
- Schilmiller AL, Moghe GD, Fan P, Ghosh B, Ning J, Jones AD, Last RL. 2015. Functionally divergent alleles and duplicated loci encoding an acyltransferase contribute to acylsugar metabolite diversity in *Solanum* trichomes. The Plant Cell **27**, 1002–1017.
- Schwaiger M, Rampler E, Hermann G, Miklos W, Berger W, Koellensperger G. 2017. Anion-exchange chromatography coupled to high-resolution mass spectrometry: a powerful tool for merging targeted and non-targeted metabolomics. Analytical Chemistry 89, 7667–7674.
- **Schwechheimer SK, Becker J, Peyriga L, et al.** 2018. Improved riboflavin production with *Ashbya gossypii* from vegetable oil based on ¹³C metabolic network analysis with combined labeling analysis by GC/MS, LC/MS, 1D, and 2D NMR. Metabolic Engineering **47**, 357–373.
- **Shastri AA, Morgan JA.** 2007. A transient isotopic labeling methodology for ¹³C metabolic flux analysis of photoautotrophic microorganisms. Phytochemistry **68**, 2302–2312.
- **Simpson JP, Olson J, Dilkes B, Chapple C.** 2021. Identification of the tyrosine- and phenylalanine-derived soluble metabolomes of Sorghum. Frontiers in Plant Science **12**, 714164.
- **Subbaraj AK, Huege J, Fraser K, Cao M, Rasmussen S, Faville M, Harrison SJ, Jones CS.** 2019. A large-scale metabolomics study to harness chemical diversity and explore biochemical mechanisms in ryegrass. Communications Biology **2**, 87.
- **Szecowka M, Heise R, Tohge T,** *et al.* 2013. Metabolic fluxes in an illuminated *Arabidopsis* rosette. The Plant Cell **25**, 694–714.
- Tian Z, Zhao R, Tolić N, Moore RJ, Stenoien DL, Robinson EW, Smith RD, Paša-Tolić L. 2010. Two-dimensional liquid chromatography system for online top-down mass spectrometry. Proteomics 10, 3610–3620.
- **Toya Y, Ishii N, Nakahigashi K, Hirasawa T, Soga T, Tomita M, Shimizu K.** 2010. ¹³C-metabolic flux analysis for batch culture of *Escherichia coli* and its *Pyk* and *Pgi* gene knockout mutants based on mass isotopomer distribution of intracellular metabolites. Biotechnology Progress **26**, 975–992.
- **Tsogtbaatar E, Cocuron JC, Alonso AP.** 2020. Non-conventional pathways enable pennycress (*Thlaspi arvense* L.) embryos to achieve high efficiency of oil biosynthesis. Journal of Experimental Botany **71**, 3037–3051.
- U.S. Food and Drug Administration, 2018. Bioanalytical method validation guidance for industry. Silver Spring, MD: U.S. Department of Health and Human Services, U.S. Food and Drug Administration.
- Vallarino JG, de Abreu E Lima F, Soria C, Tong H, Pott DM, Willmitzer L, Fernie AR, Nikoloski Z, Osorio S. 2018. Genetic diversity of strawberry germplasm using metabolomic biomarkers. Scientific Reports 8, 14386.

van Dam JC, Eman MR, Frank J, Lange HC, van Dedem GWK, Heilnen SJ. 2002. Analysis of alvcolytic intermediates in Saccharomyces cerevisiae using anion exchange chromatography and electrospray ionization with tandem mass spectrometric detection. Analytica Chimica Acta 460, 209-218

Vanhercke T. Divi UK. El Tahchy A. et al. 2017. Step changes in leaf oil accumulation via iterative metabolic engineering. Metabolic Engineering 39,

Walter TH, Blaze MTM, Boissel C. 2021. Electrospray ionization mass spectrometry ion suppression/enhancement caused by column bleed for three mixed-mode reversed-phase/anion-exchange high-performance liquid chromatography columns. Rapid Communications in Mass Spectrometry **35**, e9098.

Wang J. Christison TT. Misuno K. Lopez L. Huhmer AF. Huang Y. Hu S. 2014. Metabolomic profiling of anionic metabolites in head and neck cancer cells by capillary ion chromatography with Orbitrap mass spectrometry. Analytical Chemistry 86, 5116-5124.

Watanabe K, Nagao M, Toh R, et al. 2021. Critical role of glutamine metabolism in cardiomyocytes under oxidative stress. Biochemical and Biophysical Research Communications 534, 687-693.

Weissmann S, Ma F, Furuyama K, Gierse J, Berg H, Shao Y, Taniguchi M, Allen DK, Brutnell TP. 2016. Interactions of C₄ subtype metabolic activities and transport in maize are revealed through the characterization of DCT2 mutants. The Plant Cell 28, 466-484.

Wu S, Tohge T, Cuadros-Inostroza Á, et al. 2018. Mapping the Arabidopsis metabolic landscape by untargeted metabolomics at different environmental conditions. Molecular Plant 11, 118-134.

Xhaferaj M, Naegele E, Parr MK. 2020. Ion exchange in supercritical fluid chromatography tandem mass spectrometry (SFC-MS/MS): application for polar and ionic drugs and metabolites in forensic and anti-doping analysis. Journal of Chromatography A 1614, 460726.

Xu Y, Fu X, Sharkey TD, Shachar-Hill Y, Walker ABJ. 2021. The metabolic origins of non-photorespiratory CO2 release during photosynthesis: a metabolic flux analysis. Plant Physiology 186, 297-314.

Zhao R, Ding SJ, Shen Y, Camp DG 2nd, Livesay EA, Udseth H, Smith RD. 2009. Automated metal-free multiple-column nanoLC for improved phosphopeptide analysis sensitivity and throughput. Journal of Chromatography B 877, 663-670.

Zhou W, Yang S, Wang PG. 2017. Matrix effects and application of matrix effect factor. Bioanalysis 9, 1839-1844.